

Computer simulation of the diffusivity of cement-based materials

E. J. GARBOCZI, D. P. BENTZ

National Institute of Standards and Technology, Building Materials Division (226/B348), Gaithersburg, Maryland 20899, USA

A digital image-based model of the microstructure of cement paste, coupled with exact transport algorithms, is used to study the diffusivity of Portland cement paste. The principal variables considered are water:cement ratio, degree of cement hydration and capillary porosity. Computational methods are described and diffusivity results are presented, which are found to agree with the available experimental measurements within experimental error. Model cement pastes prepared with different water:cement ratios, and having different degrees of hydration, are found to have diffusivities that lie on a single master curve when plotted as a function of capillary porosity. Concepts from percolation theory are used to explain quantitatively the dependence of diffusivity on capillary porosity. The effect of silica fume addition on diffusivity is also examined.

1. Introduction

The transport properties of porous materials have been a subject of scientific interest for many years, and have become the focus of much attention in the last 10–20 years, primarily due to work carried out in the oil-well logging and exploration community on porous sedimentary rocks. There the interest has been in predicting transport coefficients based on microstructural parameters of the pore space. These transport coefficients include the electrical conductivity of the pore space [1], the diffusivity of the pore space (which is related to the conductivity through an Einstein relation [2, 3], and the fluid permeability [4].

Cement-based materials are porous materials whose transport coefficients are of interest, but for different reasons than for rocks. The focus of interest in rocks has been fluid permeability, which is not unreasonable as oil is a fluid that must be pumped through and out of the porous rocks in which it is found. In cement-based materials, the transport of dissolved chemical species through the pore space is of more significance, for the following reasons. Firstly, most of the physicochemical processes that degrade cement-based materials and ultimately determine service life depend on a supply of ionic species from external sources [5]. The rate at which these species can move through the pore structure largely determines the rate at which degradation proceeds. Examples include chloride ions attacking reinforcing steel in concrete, and sulphate ions reacting with aluminate phases in concrete to produce crack-causing internal expansive pressures [6]. Secondly, there has been much recent interest in using cement-based materials to contain low- and intermediate-level radioactive and also toxic waste [7]. The transport coefficients of these materials are the key factors that will determine their effectiveness as barriers.

Although both fluid permeability and ionic diffusivity are important transport coefficients for cement-based materials, this paper focuses on the diffusivity. A digital image-based growth model of the developing microstructure of cement paste during hydration is coupled with two algorithms for computing the conductance of random conductor networks, in order to carry out the computations to be described below. Preliminary accounts of some of this work have appeared previously [8, 9].

2. Digital image-based microstructural model

2.1. Cement hydration

The microstructure of cement paste is known to be complex [10]. This is not surprising, as cement paste is formed from a disordered aqueous suspension of irregularly shaped cement particles, which undergo random growth due to hydration reactions. Since the original cement particles have a wide size distribution and an average size of 15–20 μm [11], the complex microstructure of cement paste extends over many length scales, from small fractions of a micrometre to tens of micrometres.

Neglecting chemical details (which admittedly is an over simplification) the reactive growth process that cement particles undergo to produce cement paste can be thought of in the following simple way [12]. The solid cement particles supply calcium ions to the surrounding water through dissolution of surface layers. These ions then react with silica-rich surfaces of cement particles to form solid reaction products (surface products) covering the cement particles, or spontaneously nucleate in the pore space to form crystals (pore products), which can then grow further by accretion. In cement paste, the main surface product,

calcium silicate hydrate, is denoted C-S-H, and the main pore product, calcium hydroxide, is denoted CH, where the usual cement chemistry shorthand notation is C = CaO, S = SiO₂, H = H₂O, A = Al₂O₃, and F = Fe₂O₃.

The reason that cement hydration can produce a rigid solid from a viscous suspension of cement particles in water is that the hydration reaction products have a larger volume than the solid reactants. As the hydration process is nearly a constant total volume process, the reaction products can fill in the initially water-filled pore space, eventually forming a rigid solid backbone capable of bearing mechanical loads. It is convenient to define the following volume ratios. β_s is the ratio of the volume of surface products produced to the volume of cement reacted; and β_p is the analogous ratio for the pore products. The total volume expansion factor is defined as $\beta_T = \beta_s + \beta_p$. Typical ranges for these parameters, for various types of Portland cements, are $1.6 < \beta_s < 1.9$, and $0.4 < \beta_p < 0.7$ [13]. These parameters include the reaction of tricalcium silicate (C₃S), dicalcium silicate (C₂S), and the less abundant aluminate phases. The very small amount of ferrite phases present in cement was ignored in [13]. Somewhat surprisingly, for a variety of cements, the value of β_T is fairly constant, around 2.3 ± 0.1 [13]. In the simulation model to be described next, β_s is taken to be 1.7, and β_p is taken to be 0.61, so that $\beta_T = 2.31$. These particular values are those realized in the hydration of pure C₃S cement [14].

2.2. Microstructural model

In the last decade, a number of random growth or aggregation models have been developed. These models, which employ very simple random growth rules, have been shown to produce complex aggregated structures, often with fractal morphology. Two examples are the diffusion-limited aggregation (DLA) [15] and Eden models [16]. In the light of these models, it is not unreasonable to suggest that the complex microstructure of cement paste might be simulated using a few relatively simple growth rules, which are repeated many times. The model used in this paper represents a realization of this approach.

The model operates on square or cubic arrays of pixels, typically of edge length equal to 500 pixels in 2D, and 100 pixels in 3D, where each pixel is assigned to a single phase, such as pore space or cement. Initially, a specified number of cement particles (≈ 2000 in 3D) are randomly placed in the unit cell such that no two particles overlap, simulating the mixing process. Periodic boundary conditions are used to eliminate any artificial edge effects at the cell walls. The particles may be from any size distribution, within the resolution limits of the unit cell (1–100 pixels). Model particle shapes, like circles in 2D or spheres in 3D, may be used, but since the model is based on a digital image representation of the cement particles, digitized micrographs of actual particle shapes can also be used as a starting point in 2D. All the simulations described in this paper are 3D simulations.

The model operates by the iteration of cycles. Each cycle consists of three steps: dissolution, diffusion, and reaction. Fig. 1 describes the growth process schematically.

In the dissolution step, any cement pixels in contact with a water-filled pore-space pixel attempt to take a step in a random direction. The pixels whose step lands them in the pore space dissolve, and each such pixel turns into a random diffuser. The pixels whose random step would land them in a solid phase are not allowed to move, and so remain at their original location, undissolved. The number of pixels that dissolve are counted, and the correct number of extra diffusing pixels are added at random locations within the pore system, replacing pore space pixels, to account for the correct amount of surface and pore product formation. More precisely, if n pixels dissolve from off the cement surfaces, $\beta_p n$ pore product and $(\beta_s - 1)n$ extra surface product-diffusing pixels are added to the system at random locations in the pore space, in order to achieve the correct volume of hydration products arising from the reaction of the n dissolved cement pixels.

During the diffusion/reaction steps, the dissolved pixels move by executing random walks throughout the pore space. Surface-product pixels continue to move in this random fashion until they encounter a cement surface, at which point they react and attach to

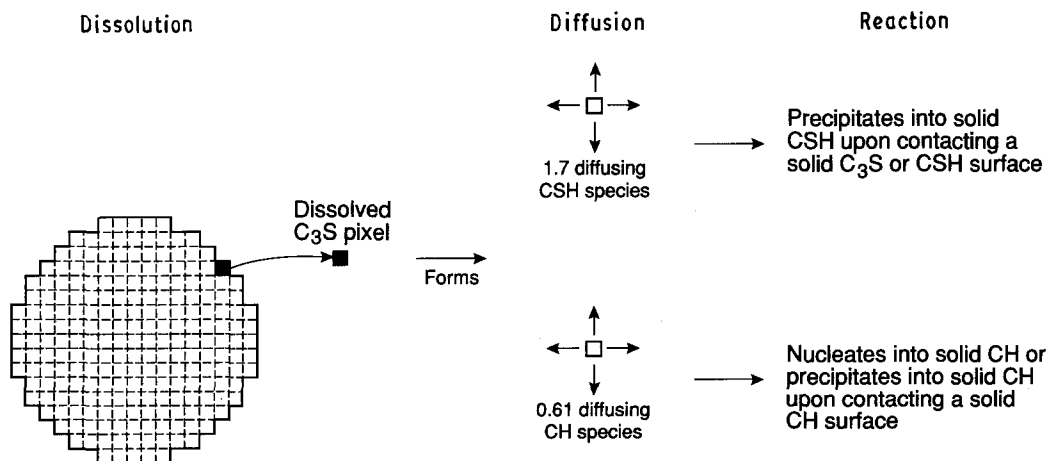


Figure 1 Schematic diagram of cement paste microstructural development algorithm.

this surface. Once surface products are present, diffusing surface-product pixels can react and attach to these surfaces as well. For any given step taken by a diffusing pore-product pixel, however, there is a non-zero probability that it can nucleate at its present location. This probability decreases exponentially as the number of diffusing pore-product pixels decreases [17]. After a pore-product cluster has been nucleated, other diffusing pore-product pixels can aggregate on to the cluster upon contact. When all diffusing pixels have reacted or nucleated, the cycle is complete, and the next cycle begins with a new dissolution step. Microstructural development is complete when all cement pixels have reacted, or when all remaining cement pixels are covered by surface product, and therefore are no longer available for dissolution. In 3-d simulations, usually up to 90% of the original cement can be hydrated using these simple rules.

The degree of hydration achieved after any completed cycle is determined from analysis of the microstructure. Degree of hydration, α , is defined as the fraction of the original cement that has been reacted, so that α equals 0 when the cement particles are first mixed with water, and attains a value of unity when hydration is complete. Another parameter that is easily calculated in the model is the water:cement (w/c) ratio, which is the weight ratio of water to cement in the initial cement-water mixture, a parameter often quoted in the cement literature. If f is the solid volume fraction, and $1 - f$ is the water volume fraction, then the water:cement ratio is given by

$$\frac{w}{c} = \frac{1 - f}{3.2f} \quad (1)$$

where 3.2 is the specific gravity of portland cement. The original porosity of a cement/water mixture, defined as the volume fraction of pore space, is then also equal to f .

3. Percolation properties of the pore space

As cement hydration progresses, the pore space is gradually being filled because the factor β_T is greater than one. The connectivity of the pore space as a function of hydration is a percolation problem. In this paper the term 'pore space' refers to capillary pore space, the water-filled space between the cement particles and their reaction products that is left over from the original cement-water mixture. There are micropores in the C-S-H surface product material, which form continuous pathways called 'gel pores'. However, transport properties are dominated by the much larger capillary pores as long as they percolate, i.e. form a continuous pathway. If the capillary pores close off, however, then transport must be dominated by the much smaller C-S-H gel micropores. There is no sharp size cut-off between capillary and gel pores. The capillary pores are considered to have a size ranging from hundreds of micrometres down to tens of nanometres, with the upper end of the C-S-H gel pore-size distribution overlapping the lower end of the capillary pore size range [11].

Since the microstructural model is represented as a digital image, there is an underlying lattice in the structure of the model. Therefore all the computational techniques developed for lattice percolation problems can be carried over to analyse digitized continuum structures like the cement paste model. For instance, the fraction of the pore space that is part of the percolating cluster is easily determined using a 'burning algorithm' [18].

Recent work using the microstructural model [13] has shown that the capillary pore space of cement paste does have a percolation threshold, at a capillary porosity ϕ of about 18%, or $\phi_c = 0.18$. This threshold ϕ_c is independent of the initial porosity or water:cement ratio [13]. Also, the C-S-H surface product phase itself has a percolation threshold, and changes from discontinuous to continuous at a volume fraction of about 17%. The close agreement of the two thresholds with a conjecture by Scher and Zallen [19, 20] as to the value of a 'universal' continuum percolation threshold of 16% in 3D has been noted and discussed [13]. For typical w/c ratios, the C-S-H phase percolates quite early in the hydration process, and is continuous simultaneously with the capillary pore space.

The percolation theory-based description of the dependence of diffusivity on cement paste microstructure will be discussed more fully in section 6.

4. Computational methods

4.1. Problem definition

The problem being considered is that of a completely water-saturated porous hardened cement paste. A concentration gradient of dissolved ions exists across the sample, so that there is a net diffusive flow of ions through the water-saturated pore space. A steady state in regard to any adsorption-desorption phenomena is assumed to have been established, so that the net flow is truly diffusive, and independent of time [3]. Under these conditions, the Nernst-Einstein relation connects the electrical conductivity of the material with its diffusivity [2, 3]. Fig. 2 illustrates the physical content of this relation. If D_0 is the diffusivity of the ions being considered in free water, and σ_0 is the conductivity of the solution in the pore space, then the result of the Nernst-Einstein relation is that

$$\frac{D}{D_0} = \frac{\sigma}{\sigma_0} \quad (2)$$

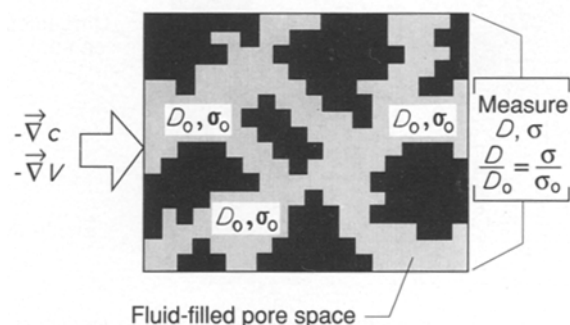


Figure 2 Schematic diagram of the physical content of the Nernst-Einstein relation relating the diffusivity and electrical conductivity of a porous material.

where D and σ are the measured diffusivity and electrical conductivity of the fluid-saturated material. Diffusion coefficients can be measured experimentally by the application of a concentration gradient, $-\nabla c$, and electrical conductivities by the application of a potential gradient, $-\nabla V$. The quantity D/D_0 is also sometimes called the diffusibility [3], or the relative diffusivity [8]. The latter term is used in this paper.

4.2. Random conductor network

The computational approach taken in this paper is to exploit the relationship given in Equation 2, by converting the digital-image model into a random conductor network, and then computing the conductivity using one of two conductivity algorithms that were developed for simple lattice problems.

The method of converting the digital-image model into a conductor network is as follows, and is illustrated schematically in Fig. 3, which shows the resulting conductor network superimposed on an original random 2D image. After a digital image cement paste model is generated, a 1 pixel-thick electrode is 'glued' on opposing faces of the unit cube. A network of nodes is created, with one node at the centre of each pixel. Conductors with conductance Σ_{ij} are then set up which connect the nodes in nearest-neighbour pixels i and j , which themselves have conductivities σ_i and σ_j , respectively. The conductance Σ_{ij} is defined as the series combination of Σ_i and Σ_j

$$\Sigma_{ij} = \frac{1}{1/\Sigma_i + 1/\Sigma_j} \quad (3)$$

where Σ_i is the conductance of one half of pixel i . This means that $\Sigma_i = \sigma_i d^2/(0.5d) = 2 \sigma_i d$, where d is the edge length of one pixel. If pixels i and j are both capillary pore space pixels, for example, then $\sigma_i = \sigma_j = 1$, so that $\Sigma_{ij} = d$. If either pixel i or pixel j is a cement or pore-product pixel, then $\Sigma_{ij} = 0$, since either σ_i or σ_j is zero.

The surface-product (C-S-H) pixels are taken to have a small non-zero conductivity, because of the

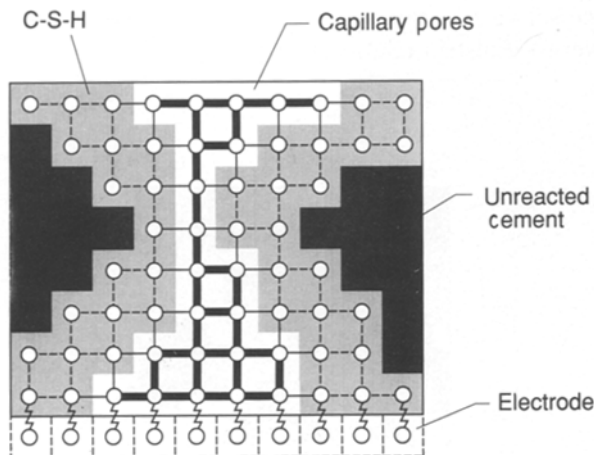


Figure 3 Schematic diagram of the digital image to random conductor network mapping used to compute the electrical conductivity of the cement paste model. Conductances of the different types of bonds are given in the text.

surface product's continuous gel micropores. The diffusivity results were all obtained using $\sigma_{C-S-H} = 0.0025$, which was based on experimental data from chloride ion diffusivity measurements [3, 21]. Assigning a bulk conductivity to the C-S-H phase is an approximation, since these pores are so small that the flow of diffusing ions or the movement of charged particles in them probably differs greatly from bulk processes [3], and thus depends on the ion considered. For example, it is known that caesium (Cs^+) ion diffusivities are systematically smaller than chloride ion diffusivities measured in the same material [3], so a different value for σ_{C-S-H} would be needed to describe caesium-ion diffusion. A conductor connecting a C-S-H pixel node to a capillary pore-space node is then given a conductance of $d/200.5$, in accordance with Equation 3. The electrodes are considered to have infinite conductivity, which results in the value of Σ_{ij} being $2\sigma_j d$ when pixel i is on the electrode, and pixel j has finite conductivity σ_j .

Figure 3 shows the five different values of conductances used. No connection indicates a zero conductance. The thin dashed lines are $0.0025d$, the thin solid lines are $d/200.5$, and the thick solid lines have conductances d . The zig-zag line denotes a conductor-electrode connection, having a conductance of either $2d$ or $2(0.0025)d$, for a capillary or a C-S-H pixel connected to the electrode, respectively.

4.3. Conductance algorithms

Once the conductor network is built, its effective conductance is computed using one of two efficient methods. If the average connectivity of the nodes is small enough, around 1.5 bonds per node on average, then the Fogelholm algorithm can be used. This algorithm was first written in LISP by Fogelholm [22] for 2D problems, and was recently extended to three- and higher-dimensional problems using a program written in C [23]. This algorithm systematically reduces the network down to two nodes, with the conductance of the last remaining conductor being the equivalent conductance of the entire network. It is very efficient, partly because the equivalent conductivity is obtained without having to solve for the electric potential at every point. However, the speed of the algorithm decreases extraordinarily with the average number of connections per node. In Reference 23, the problem considered was the computation of the conductivity close to the percolation threshold, $p_c = 0.249$, where p is the fraction of bonds remaining, for bond percolation [18] on the simple cubic lattice. However we have found that the algorithm becomes unacceptably slow for $p > 0.29$ for the same problem solved on a 100^3 cubic lattice.

The Fogelholm algorithm is still useful for the cement paste problem, since there are many ranges of porosity which yield an effective p in the right range. However, most of the results reported in this paper were obtained using a second algorithm, a conjugate gradient relaxation algorithm [24].

The conjugate gradient relaxation algorithm essentially solves the complete electrical problem of the

voltage distribution in a random material across which a potential difference is applied. The output of the algorithm is the voltage at every node, from which the total current and thus equivalent conductance is calculated. The input is an initial voltage distribution, usually taken to be 1 and 0 at the two electrodes, and linearly interpolated at nodes in between. The voltages are then cyclically updated until Kirchoff's laws are satisfied at each node within some preset finite precision [24]. At low porosities, the conjugate gradient algorithm is slower than the Fogelholm algorithm, as it gives all the voltage information as well as the equivalent conductance, but it can handle any degree of connectivity and eventually becomes the faster algorithm, as the Fogelholm algorithm's speed decreases much more rapidly with increasing porosity.

5. Diffusivity results

5.1. Plain cement paste results

We have simulated the relative diffusivity D/D_0 for 0.4, 0.45, 0.5, and 0.6 w/c ratio cement pastes, as a function of degree of hydration, α . The results, obtained using 100^3 pixel unit cells, are plotted in Figs 4–7, along with reported experimental data [3, 21, 25]. It should be noted that the total computer time used for all the results described in this paper was on the order of 100 h on a single processor, Convex C120 mini-supercomputer. All simulations were run using 32-bit precision real numbers, with no significant difference between 32- and 64-bit precision runs.

In Figs 4–7, the open squares are simulation results and the filled circles the experimental results. One initial cement-particle packing was used at each w/c ratio to generate the simulation results. The fairly small (at most 10–20%) variation between different initial cement-particle packings is less than the expected error in the experimental results, so that it was not worth averaging over several configurations. There is reasonably good agreement between simulations and experiment.

In Figs 6 and 7, however, there is one experimental data point that is significantly different (by a factor of 2 or 3) from the simulation results. The experimental data points did not have a measured degree of hydra-

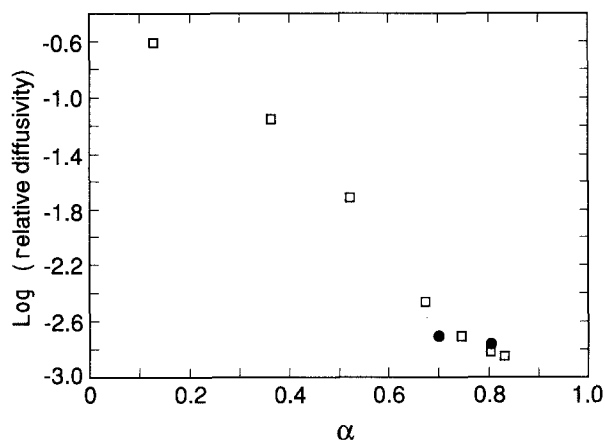


Figure 4 Logarithm (base 10) of the relative diffusivity, D/D_0 , against degree of hydration, α , for (□) simulation and (●) experiment for a 0.4 w/c cement paste.

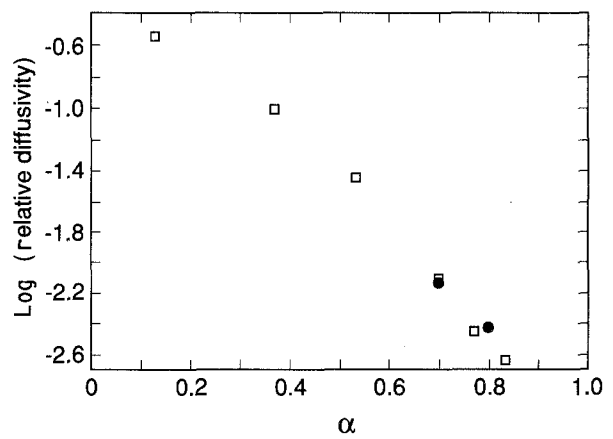


Figure 5 Logarithm (base 10) of the relative diffusivity, D/D_0 , against degree of hydration, α , for (□) simulation and (●) experiment for a 0.45 w/c cement paste.

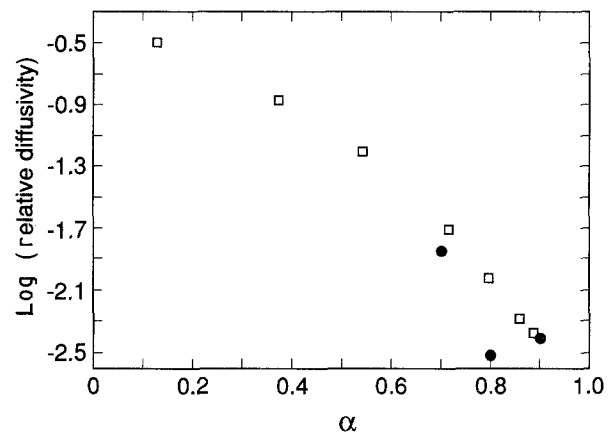


Figure 6 Logarithm (base 10) of the relative diffusivity, D/D_0 , against degree of hydration, α , for (□) simulation and (●) experiment for a 0.5 w/c cement paste.

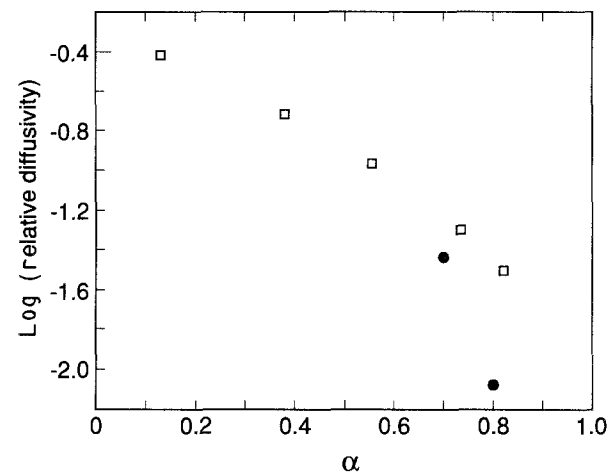


Figure 7 Logarithm (base 10) of the relative diffusivity, D/D_0 , against degree of hydration, α , for (□) simulation and (●) experiment for a 0.6 w/c cement paste.

tion, as only their ages were recorded. Consequently the degree of hydration was estimated as follows. The 28-day-old samples measured in Reference 3 were assigned $\alpha = 0.7$, the 60-day-old samples measured in Reference 21 were assigned $\alpha = 0.8$, and the 180-day-old samples measured in Reference 25 were assigned α

= 0.9. These values of α were not picked to give the best agreement with simulation, but rather were based on data presented in Reference 11. This correlation between α and age was assumed to be independent of w/c ratio. However, it is known that higher w/c ratio cement pastes can hydrate faster than lower w/c ratio pastes [26], so that the apparent disagreement in Figs 6 and 7 could just be due to an incorrectly assigned degree of hydration. In all fairness, it should be stated that this caveat also applies to the points that agreed well with the simulation results.

5.2. Silica fume results

Condensed silica fume (a small, 0.2–0.4 μm , highly reactive, almost pure amorphous silica material) is being increasingly used as a mineral admixture in concrete where a low chloride diffusivity is desired [27]. Its effect on transport properties in concrete or mortar is probably partly due to modification of the sand–cement paste interfacial zone [10, 28], and partly to modification of bulk cement paste microstructure [13]. Bentz and Garboczi [13] showed how the incorporation of silica fume into the cement paste could be simulated. The silica fume reacts with the CH phase to produce more (pozzolanic or secondary) C–S–H, which has a larger volume than the original CH and silica fume combined. Therefore, using silica fume tends to further reduce the capillary porosity of a cement paste relative to that of a plain paste.

The incorporation of silica fume has been simulated at two different water-to-solid (w/s) ratios, 0.6 and 0.4, where w/s ratio is defined similarly to w/c ratio in Equation 1, but with the weight of cement replaced by weight of cement plus silica fume. Cement (10 and 20 wt %) has been replaced by silica fume, which keeps the w/s ratio constant, permitting a fair comparison with plain cement paste at an equivalent w/c ratio [13]. Silica fume has a lower specific gravity than cement, so that the fraction of solid volume initially taken up by the silica fume is greater than its fraction by weight.

Fig. 8 shows the simulated diffusivity results for 0, 10 and 20% replacement of the cement by silica fume, for $w/s = 0.60$. The 0% data are the same as shown in

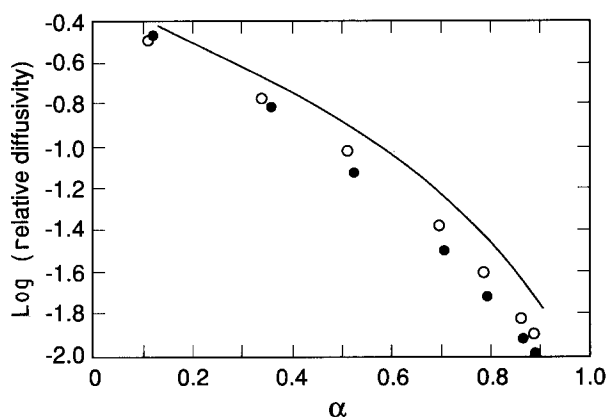


Figure 8 Logarithm (base 10) of the relative diffusivity, D/D_0 , against degree of hydration α , for a 0.6 w/s (water to solid) cement paste, in which (●) 10 and (○) 20 wt % of the cement has been replaced by condensed silica fume. (—) 0% silica fume.

Fig. 7, connected with straight-line segments to facilitate comparison with the silica fume results, which do not lie at exactly the same degrees of hydration. Both the 10 and 20% results lie below the 0% diffusivities, which is as expected since the reaction of silica fume with CH reduces the capillary porosity. However, it is a little surprising that the 10% silica fume pastes have a lower diffusivity at all degrees of hydration past 0.2 than the 20% silica fume results. This result can be easily explained by studying Fig. 9. In this Figure, capillary porosity against weight percentage silica fume, taken as a percentage of total original solid weight, is plotted for various degrees of hydration, using relationships developed in Reference 13, for $w/s = 0.60$. The $\alpha = 0.2$ curve shows that the capillary porosity is almost identical for 10 and 20% silica fume replacement, which is the reason that the two diffusivities in Fig. 8 at $\alpha = 0.12$ are almost identical. For $\alpha > 0.2$, though, the capillary porosity is always smaller for the 10% than for the 20% silica fume pastes. Physically, this is because there is a trade-off when replacing cement with silica fume. Less cement means that there will be less CH produced to react with the silica fume. At small silica fume fractions, there is more than enough CH to react with all the silica fume, but as cement content decreases and silica fume content increases, there comes a point when there is too much silica fume to react with the CH produced, and part of the silica fume begins to act as an inert filler which cannot fill pore space as effectively as reactive cement [13]. This is the physical explanation for the minima in the plots shown in Fig. 9. It should also be noted that the greatest differences in diffusivity between the 10 and 20% results are at intermediate degrees of hydration, $0.4 < \alpha < 0.6$, where the greatest differences in capillary porosity are also found in Fig. 9.

This explanation suffices for the $w/s = 0.60$ data, as the capillary pore space always remains continuous, so that the relative diffusivity is always dominated by the capillary pore space. Differences in capillary porosity are then directly and easily related to differences in relative diffusivity. However, the $w/s = 0.40$ results are somewhat different, because the capillary porosity falls below $\phi_c = 0.18$.

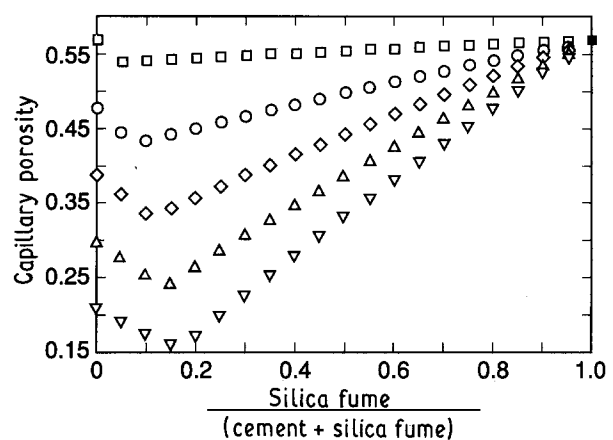


Figure 9 Capillary porosity against percentage of total original solids, by weight, of silica fume mixed with the original cement at $w/s = 0.6$, for various degrees of hydration: □, 0.2; ○, 0.4; ◇, 0.6; △, 0.8; ▽, 1.0.

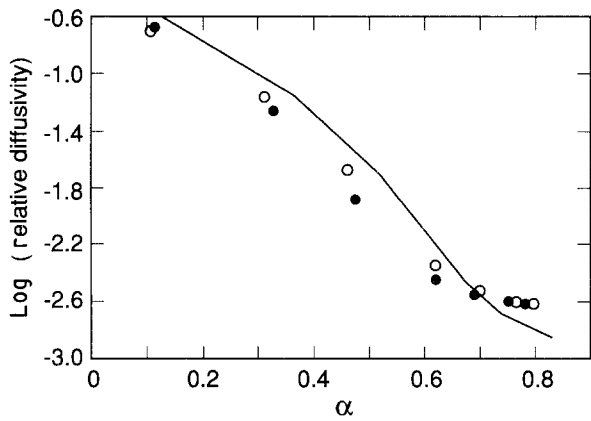


Figure 10 Logarithm (base 10) of the relative diffusivity, D/D_0 , against degree of hydration α , for a 0.4 w/s (water to solid) cement paste, in which (●) 10 and (○) 20 wt % of the cement has been replaced by condensed silica fume. (—) 0% silica fume.

Fig. 10 shows the diffusivity results for a w/s ratio of 0.40. Again, the 10% silica fume pastes have about the same diffusivity as the 20% silica fume pastes at the lowest degrees of hydration. The 0% silica fume data is from Fig. 4. For intermediate degrees of hydration, the 10% results are systematically lower. Fig. 11 shows the capillary porosity plotted as a function of silica fume weight fraction for the 0.4 w/s ratio pastes, which explains the intermediate degree of hydration results of Fig. 10, in the same way as Fig. 9 explained the results of Fig. 8. For degrees of hydration greater than 0.6, however, the 10 and 20% silica fume results converge to the value $D/D_0 = 0.0025$ ($\log_{10}(0.0025) = -2.6$), and are systematically above the plain cement paste results. This is because if there is enough silica fume to convert basically all the CH to secondary C-S-H, at high degrees of hydration where there is very little unreacted cement or capillary pore space left, the cement paste will consist almost entirely of C-S-H. The C-S-H phase has been modelled as having a relative diffusivity of 0.0025, so that the bulk value of relative diffusivity for the paste will be the same. For lesser amounts of silica fume replacement, so that not all the CH is reacted, the minimum value of

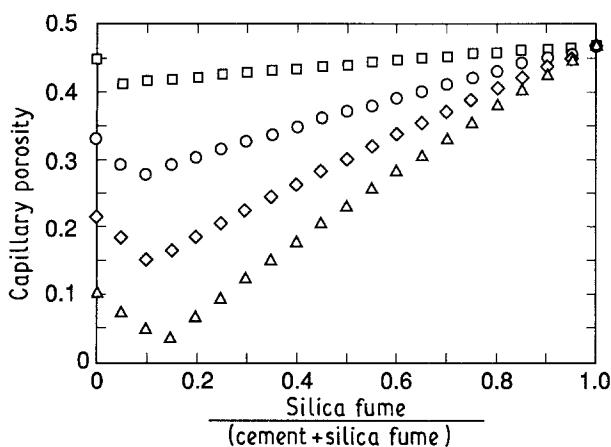


Figure 11 Capillary porosity against percentage of total original solids, by weight, of silica fume mixed with the original cement, at w/s = 0.4, for various degrees of hydration; □, 0.2; ○, 0.4; ◇, 0.6; △, 0.8.

D/D_0 will vary continuously between 0.001, the minimum for plain cement paste (to be derived in Section 6.3), and 0.0025, the value obtained for complete reaction of cement and CH.

The above results imply that silica fume replacement of cement can reduce the diffusivity of bulk cement paste by reducing the capillary porosity, but at low porosities and high degrees of hydration, silica fume replacement can actually increase diffusivity by replacing impervious CH with microporous C-S-H. Silica fume in concrete could also reduce the diffusivity by reducing the porosity of the sand-cement paste interfacial zone, if transport through the concrete were dominated by pathways connecting through the interfacial zone regions.

An additional possibility not considered in this work is that silica fume modifies the microstructure of the C-S-H gel phase, changing its effective diffusivity relative to the C-S-H in plain paste. Reductions in the C/S ratio of the C-S-H, from 1.7 to 1.4, have been observed in cements containing pozzolanic admixtures like silica fume [29, 30], as well as an increase in the polymerization of the C-S-H gel phase [31]. These structural changes could mean that a different effective bulk diffusivity should be assigned to the C-S-H phase in cement pastes containing silica fume. An additional difficulty exists when comparing equal age specimens of silica fume-modified cement paste, as is usually done, in that silica fume may accelerate the hydration process [31], so that specimens of the same age, but with different amounts of silica fume, may have different degrees of hydration. Thus the presence of silica fume may modify the relationship between age and degree of hydration used above.

6. Cement paste diffusivity dependence on pore structure

6.1. Capillary porosity contribution

Since the microstructural model gives a detailed quantitative picture of the cement paste pore structure at any degree of hydration, it can be used to determine the dependence of diffusivity on pore structure in a fundamental way.

Of the two phases that contribute to the diffusivity, the capillary pore space and the C-S-H gel phase, the capillary pore space is first considered. The capillary pore space percolation threshold occurs when the capillary porosity is 18%, expressed as a percentage of total volume. For porosities well above this threshold, the diffusivity should be dominated by the capillary pore space, since its conductivity is so much higher (by a factor of 400) than the C-S-H, although the C-S-H contribution is still not totally negligible. To separate the contributions of the two phases, the diffusivity was computed with $\sigma_{C-S-H} = 0$ [8]. The diffusivity of course then tends towards 0 as the capillary porosity approaches the percolation threshold of 18%. In Fig. 12, the logarithm of diffusivity is plotted against the logarithm of the quantity $(\phi - 0.18)$, where ϕ is the capillary porosity. From percolation theory, it is expected that such a plot will result in a straight line with a slope of about $t = 2$ [22] as ϕ approaches $\phi_c = 0.18$,

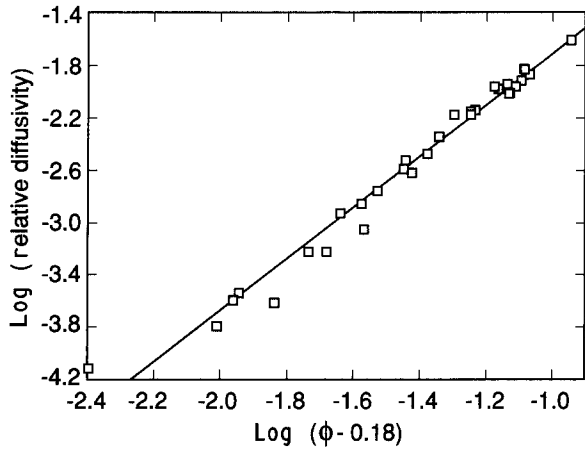


Figure 12 Plot of $\log_{10}(D/D_0)$ against $\log_{10}(\phi - \phi_c)$, where ϕ is the capillary porosity, and $\phi_c = 0.18$ is the approximate percolation threshold for the capillary pore space [13]. The solid curve is a best-fit straight line, and the simulation data points were obtained using the Fogelholm algorithm [21]. No C-S-H contribution to transport.

since the diffusivity is expected to scale as $(\phi - 0.18)^2$ in this region [18]. This scaling is expected from the concept of the universality of critical transport exponents [18]. A very good straight line is indeed found, with the correct slope of about 2.0. The complete equation of the line is

$$\frac{D}{D_0} = 1.8 (\phi - 0.18)^2 \quad (4)$$

based on a least-squares fit. Even though this functional form is required to hold only for ϕ near ϕ_c , it is known usually to hold farther away as well [32], so that Equation 4 is adopted to characterize the connected fraction of the capillary pore space's contribution to diffusivity for all $0.18 < \phi < 0.60$. Fig. 12 demonstrates that this functional form does indeed hold rather far away from $\phi_c = 0.18$.

6.2. C-S-H contribution

When the capillary porosity falls below 18%, then the diffusivity will be controlled by transport through C-S-H gel pores. However, there is still some capillary pore space left, in the form of isolated clusters. The physical picture of the dominant diffusive flow pathways in this regime consists of isolated capillary pore clusters linked together by C-S-H gel pore pathways. Although the C-S-H phase is itself continuous, pathways that also include the much more conductive capillary pores should be more important to the total diffusivity. This physical picture is similar to that proposed by Atkinson and Nickerson [3]. Capillary porosity, ϕ , will still be an appropriate variable in this regime, with the diffusivity continuing to decrease with ϕ . For $\phi < 0.18$, then, the diffusivity is fitted with an Archie's law [33] form, $a\phi^m$, with a and m constants, but modified by having a cut-off value R_{\min} , where R_{\min} is the value of the relative diffusivity when the capillary porosity is zero. For sandstone rocks, for

which Archie's law was defined, the critical value of the porosity is approximately zero, so that the transport properties and ϕ approach zero simultaneously [33]. (Archie's law is really of the same functional form as Equation 3, $(\phi - \phi_c)^m$, but for sandstone rocks, $\phi_c \approx 0$. Atkinson and Nickerson [3], when demonstrating that Archie's law did not apply to cement paste, did not know that $\phi_c = 0.18$, rather than 0.0, for cement paste.) However, a zero capillary porosity cement paste would be composed of C-S-H, CH, and unreacted cement, which will have a non-zero relative diffusivity R_{\min} because of the connected gel pores of the C-S-H phase. The value of R_{\min} is not a fitting parameter, but can be calculated using composite theory and the known value of ϕ_{C-S-H} , as described in Section 6.3.

If we consider the pure capillary pore-space diffusivity above $\phi = 0.18$, and the C-S-H/capillary pore-space pathways for all values of ϕ , to be roughly in parallel, then a reasonable functional form for the relative diffusivity as a function of capillary porosity, which is well justified physically, is

$$\begin{aligned} \frac{D}{D_0} &= 0.001 + a\phi^2 + H(\phi - 0.18) \\ &\quad \times 1.8 \times (\phi - 0.18)^2 \end{aligned} \quad (5)$$

where H is a function such that $H(x) = 1$ for $x > 0$, $H(x) = 0$ for $x \leq 0$, the exponent m of the Archie's law term is assumed to be 2 because of the universality of exponents mentioned above [18], and a is a parameter to be fitted to data points having $\phi < 0.18$. After this fit is carried out, Equation 5 becomes

$$\begin{aligned} \frac{D}{D_0} &= 0.001 + 0.07\phi^2 + H(\phi - 0.18) \\ &\quad \times 1.8 \times (\phi - 0.18)^2 \end{aligned} \quad (6)$$

Fig. 13 shows Equation 6 plotted along with all the simulation data points from Figs 4-7. Equation 6 gives a reasonably good description of the relative diffusivity D/D_0 over the capillary porosity range $0 < \phi < 0.6$. Equation 6 must break down at some point for $\phi > 0.6$, as it does not give the correct $\phi \rightarrow 1$ limit of $D/D_0 = 1$.

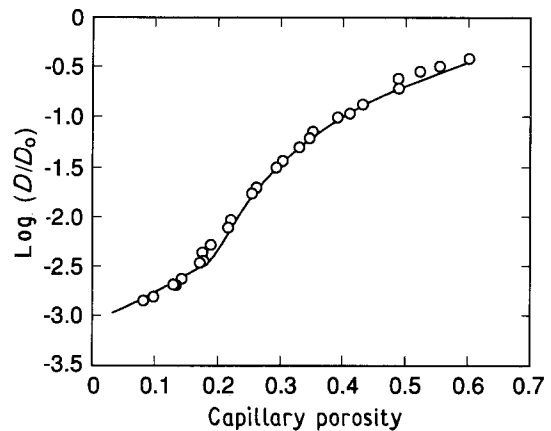


Figure 13 Logarithm (base 10) of the relative diffusivity D/D_0 against capillary porosity for all plain cement paste simulation data points. The solid line is given by Equation 6.

6.3. Zero porosity diffusivity derivation

The cut-off value of the plain cement paste relative diffusivity at $\phi = 0$ of 0.001 is justified by the use of a recent equation that gives a percolation theory-based description of the effective conductivity of a two-component composite [34]. For plain cement paste with no silica fume, at $\phi = 0$ the two components are C-S-H, with $D/D_0 = 0.0025$, and the combination of CH and any unreacted cement, with D/D_0 assumed to be zero for this phase. The equation to be solved for the effective relative diffusivity, D_m/D_0 , for the composite is

$$Ax^2 + Bx - x_L x_H = 0 \quad (7)$$

where $A \propto (1 - v_c)/v_c$, $v_c = 0.16$ is the percolation threshold in terms of volume fraction v for C-S-H, which in this case is the high conductivity phase, $x = (D_m/D_0)^{1/t}$, $t = 2$ is the universal critical exponent for conduction/diffusion percolation problems in three dimensions [23], $x_L = 0$ is the conductivity of the low-conductivity phase, $x_H = (\sigma_{C-S-H})^{1/t} = (0.0025)^{1/t}$, and $B = x_H(1 - v - Av) + x_L(Av + v - A)$. Since $x_L = 0$, Equation 7 becomes

$$\begin{aligned} \frac{D_m}{D_0} &= (-B/A)^t = (-B/A)^2 \\ &= \frac{\sigma_{C-S-H}(1 - v - Av)^2}{A^2} \end{aligned} \quad (8)$$

For w/c ratios less than 0.41, it is theoretically possible to achieve zero capillary porosity for degrees of hydration < 1 . Using the C-S-H volume expansion factor β_s , the CH volume expansion factor β_p , and Equation 1, which relates w/c ratio and initial cement and water volume fractions, it is possible to show that the volume fractions of C-S-H and (CH + unreacted cement) at $\phi = 0$ are given in terms of w/c ratio by

$$\begin{aligned} v_{C-S-H} &= \frac{3.2\beta_s w/c}{(1 + 3.2w/c)(\beta_T - 1)} \\ v_{CH+cement} &= \frac{\beta_T - 1 + 3.2(\beta_P - 1)w/c}{(1 + 3.2w/c)(\beta_T - 1)} \end{aligned} \quad (9)$$

Using Equations 8 and 9, and $\beta_S = 1.7$ and $\beta_P = 0.61$, we find that $D_m/D_0 = R_{\min}$ equals 0.0012 for a w/c ratio 0.4, 0.00098 for $w/c = 0.35$, and 0.0008 for $w/c = 0.3$, thus justifying the choice of 0.001 as a reasonable approximation for any w/c ratio less than 0.41, when no silica fume is present. With silica fume present, a more reasonable value of the cut-off value is $0.001 < R_{\min} < 0.0025$, depending on the amount of silica fume replacement, as discussed in section 5.2 above.

7. Conclusions

In order to understand the dependence of diffusivity on the microstructure of a porous material like Portland cement paste, there must first be quantitative understanding of microstructure, as well as methods for calculating the diffusivity for a given microstructure. Both these goals have been achieved by using a random growth model for generation of the microstructure of the cement paste, and by using exact

algorithms applied to the underlying digital-image lattice of the model to calculate the diffusivity for a given microstructure. It should be emphasized that the quantitative representation of the microstructure was achieved by basing the model on a digital image, and that the transport algorithms used were only applicable to a lattice structure, as used here. The results obtained are summarized below.

1. The ionic diffusivity of cement paste can be calculated with algorithms applied to the digital image-based microstructural model, with calculated values of steady-state chloride ion diffusivities in reasonable agreement with experimental data. The calculation techniques are equally applicable to actual as to model microstructures.

2. The chloride diffusivity of plain Portland cement paste can be expressed as a function of capillary porosity only, with the functional form being $D/D_0 = 0.001 + 0.07\phi^2 + H(\phi - 0.18) 1.8 (\phi - 0.18)^2$, where $H(x) = 0$ for $x \leq 0$, and 1 for $x > 0$. This relationship is dominated by the percolation properties of the capillary pore space above the critical capillary porosity $\phi_C = 0.18$, where the capillary pore space becomes disconnected, and by simple Archie's law-type power-law behaviour below ϕ_C , where the pathways through C-S-H gel pores dominate the transport. The above functional form must break down at porosities somewhat higher than 0.6, as it does not give the correct $\phi = 1$ limit.

3. The physical picture of diffusive transport in cement paste is as follows. Above $\phi = \phi_C$, transport is mainly through continuous capillary pores, with a smaller amount of flow through pathways of capillary pores linked by C-S-H gel pores. Below ϕ_C , the dominant pathways are now made up of isolated capillary pore clusters linked together by C-S-H gel-pore connections, which determine the flow rate [3].

4. The minimum value of D/D_0 for chloride ions diffusing through plain Portland cement paste has been predicted to be about 0.001, obtained when the capillary porosity is zero. With silica fume present, the cut-off value becomes 0.0025.

5. For low w/s ratios, when sufficient silica fume is present to react with most of the CH produced, and when the capillary porosity is much less than $\phi_C = 0.18$, so that the diffusivity is controlled by the C-S-H phase, the addition of silica fume can increase the relative diffusivity by consuming CH ($D/D_0 = 0$), and replacing it with C-S-H ($D/D_0 = 0.0025$).

Acknowledgements

The authors would like to thank the National Science Foundation Science and Technology Center for Advanced Cement-Based Materials for partial support of this work; P. M. Duxbury for supplying a working copy of a 2-d conjugate gradient code; and C. J. Lobb for several helpful conversations.

References

1. L. M. SCHWARTZ and J. R. BANAVAR, *Phys. Rev. B*, **39** (1989) 11965.

2. V. K. S. SHANTE and S. KIRKPATRICK, *Adv. Phys.* **20**, (1971) 325.
3. A. ATKINSON and A. K. NICKERSON, *J. Mater. Sci.* **19** (1984) 3069.
4. A. H. THOMPSON, A. J. KATZ and C. E. KROHN, *Adv. Phys.* **36** (1987) 625.
5. J. POMMERSHEIM and J. R. CLIFTON, *Mater. Const.* **18** (1985) 21.
6. W. C. HANSON in "The Chemistry of Sulphate-Resisting Portland Cements", edited by E. G. Swanson (University of Toronto Press, Toronto, 1968).
7. A. ATKINSON, *Nucl. Chem. Mgt* **5** (1985) 203.
8. D. P. BENTZ, D. B. GINGOLD, E. J. GARBOCZI, C. J. LOBB and H. M. JENNINGS, *Ceram. Trans.* **16** (1991) 211.
9. E. J. GARBOCZI and D. P. BENTZ in "Materials Science of Concrete" Vol. II, edited by J. Skalny (American Ceramic Society, Westville, 1991) in press.
10. K. L. SCRIVENER in "Materials Science of Concrete" Vol. I, edited by J. Skalny (American Ceramic Society, Westville, 1989) p. 127.
11. S. MINDESS and J. F. YOUNG, "Concrete" (Prentice-Hall Englewood Cliffs, New Jersey, 1981) Ch. 4.
12. E. M. GARTNER and J. M. GAIDIS in "Materials Science of Concrete" Vol. I, edited by J. Skalny (American Ceramic Society, Westerville, 1989) p. 95.
13. D. P. BENTZ and E. J. GARBOCZI, *Cement Concrete Res.* **21** (1991) 325.
14. J. F. YOUNG and W. HANSEN in "Microstructural Development During Hydration of Cement", edited by L. J. Struble and P. W. Brown (Materials Research Society, Pittsburgh, 1987) p. 313.
15. P. MEAKIN, in "Phase Transitions and Critical Phenomena" Vol. 12, edited by C. Domb and J. L. Leibowitz (Academic, New York, 1988).
16. M. EDEN, in Proceedings of the Fourth Berkeley Symposium on Mathematical Statistics and Probability, Vol. IV, edited by Jerzy Neyman (University of California Press, Berkeley, 1961).
17. E. J. GARBOCZI and D. P. BENTZ, *J. Mater. Res.* **6** (1991) 196.
18. D. STAUFFER, "Introduction to Percolation Theory" (Taylor & Francis, London, 1985) Ch. 1.
19. H. SCHER and R. ZALLEN, *J. Chem. Phys.* **53** (197) 3759.
20. R. ZALLEN, "The Physics of Amorphous Solids" (Wiley, New York, 1983) Ch. 4.
21. C. L. PAGE, N. R. SHORT and A. El TARRAS, *Cement Concrete Res.* **11** (1981) 395.
22. R. FOGELHOLM, *J. Phys.* **C13**, (1980) L571.
23. D. B. GINGOLD and C. J. LOBB, *Phys. Rev. B* **42** (1990) 8220.
24. W. H. PRESS, B. P. FLANNERY, S. A. TEUKOLSKY and W. T. VETTERLING, "Numerical Recipes: The Art of Scientific Computing" (Cambridge University Press, Cambridge, 1986) Ch. 10.
25. O. GAUTEFALL, *American Concrete Institute Special Publication* 91-48.
26. J. H. TALPIN, *Aust. J. Appl. Sci.* **10** (1959) 329.
27. L. ROBERTS, in "Materials Science of Concrete" Vol. I, edited by J. Skalny (American Ceramic Society, Westerville, 1989) p. 197.
28. D. P. BENTZ and E. J. GARBOCZI, *Amer. Conc. Inst. Mater. J.* (Sept./Oct. 1991).
29. S. A. RODGER and G. W. GROVES, *Adv. Cement Res.* **1** (1988) 84.
30. Z. Q. WU and J. F. YOUNG, *J. Mater. Sci.* **19** (1984) 3477.
31. C. M. DOBSON, D. G. C. GOBERDHAN, J. D. F. RAMSAY and S. A. RODGER, *ibid.* **23** (1988) 4108.
32. M. A. DUBSON and J. C. GARLAND, *Phys. Rev. B* **32** (1985) 7621.
33. P. SEN, C. SCALA and M. H. COHEN, *Geophys.* **46** (1981) 781.
34. D. S. McLACHLAN, M. BLASZKIEWICZ and R. E. NEWNHAM, *J. Am. Ceram. Soc.* **73** (1990) 2187.

*Received 10 December 1990
and accepted 13 May 1991*